Journal of Alloys and Compounds 503 (2010) 500–506

Contents lists available at ScienceDirect

Journal of Alloys and Compounds

journal homepage: www.elsevier.com/locate/jallcom

Sonochemical synthesis of $Dy_2(CO_3)_3$ nanoparticles and their conversion to Dy_2O_3 and $Dy(OH)_3$: Effects of synthesis parameters

Masoud Salavati-Niasari[a,b,*], Jaber Javidi[a], Fatemeh Davar[a], Alireza Amini Fazl[c]

[a] Institute of Nano Science and Nano Technology, University of Kashan, P.O. Box. 87317–51167, Kashan, I.R., Iran
[b] Department of Inorganic Chemistry, Faculty of Science, University of Kashan, P.O. Box. 87317–51167, Kashan, I.R., Iran
[c] Institute for Colorants, Paint and Coatings (ICPC), P.O. Box. 16765/654, Tehran, I.R., Iran

ARTICLE INFO

Article history:
Received 29 December 2009
Received in revised form 6 May 2010
Accepted 7 May 2010
Available online 20 May 2010

Keywords:
Dysprosium carbonates
Ultrasonic
Nanoparticles
Dy_2O_3
$Dy(OH)_3$

ABSTRACT

Dysprosium carbonates nanoparticles were synthesized by the reaction of $Dy(CH_3COO)_3{\cdot}6H_2O$ and sodium hydroxide by a sonochemical method. Dysprosium oxide nanoparticles with average size about 12 nm were prepared from calcination of $Dy_2(CO_3)_3{\cdot}xH_2O$ nanoparticles. $Dy(OH)_3$ nanoparticles were synthesized by facial hydrothermal processing from Dy_2O_3 nanoparticles. The as-synthesized nanoparticles were characterized by scanning electron microscopy (SEM), X-ray powder diffraction (XRD), X-ray photoelectron spectrum (XPS), transmission electron microscopy (TEM), Fourier transform infrared spectroscopy (FT-IR) and photoluminescence (PL). The PL result showed one broad emission band centered at 390 nm (λ_{ex} = 300 nm) of the pure Dy_2O_3 nanoparticles. The role of surfactant, calcination temperature and sonication time were investigated on the morphology and particle size of the products.

1. Introduction

Nanomaterials have generated a lot of interest due to their unique physical and chemical properties that are significantly different from those of bulk materials. Reducing the particle size to a few nanometers, while keeping its chemical composition fixed, can change the fundamental properties of a material [1–5].

Rare-earth oxides have been widely used as high-performance luminescent devices, magnets, catalysts, and other functional materials based on the electronic, optical, and chemical characteristics arising from their 4f electrons [6].

Among compounds of the rare-earth family, dysprosium compounds have been synthesized via different techniques such as Hydrothermal or solvothermal [7,8], sol–gel [9] and other methods. Xu et al. have reported $Dy(OH)_3$ and Dy_2O_3 nanotubes by hydrothermal method [6]. Dysprosium hydroxide and oxide nanorods were prepared directly from commercial bulk Dy_2O_3 crystals by hydrothermal process at 130 and 210 °C, respectively, by Song et al. [10].

Sonochemical method is a facile route operated under ambient conditions. During sonication, ultrasonic sound waves radiate through the solution causing alternating high and low pressure in the liquid media. This leads to the formation, growth, and implosive collapse of bubbles in a liquid. The collapse of bubbles with short lifetimes produces intense local heating and high pressure. These localized hot spots can drive many chemical reactions [11]. In recent years, sonochemical methods have been extensively explored to synthesize various nanostructures, including particles [12], hollow spheres [13], porous spheres [14], rods [15], tubes [16], and wires [17].

The sonochemical method comparing to the other methods which have been used for preparing the $Dy_2(CO_3)_3$, Dy_2O_3 is very fast and it does not need high temperatures during the reactions, using the surfactants is not necessary for this method and the other advantage of using ultrasound radiation is that it yields smaller particles [18].

In this paper, we demonstrated that dysprosium oxide (Dy_2O_3) could be successfully prepared by a simple sonochemical method from dysprosium acetate and sodium carbonate in an ultrasonic device and it was worth noting that the size of dysprosium oxide nanoparticles could be easily controlled by adjusting the synthetic parameters. And so, we report a simple method for prepare of $Dy(OH)_3$ nanoparticles by facile hydrothermal treatment of Dy_2O_3 nanoparticles. In addition, the effects of some parameter on the formation Dy_2O_3 nanostructures were investigated. And their photoluminescence (PL) properties of Dy_2O_3 nanoparticles were discussed. We believe that this manuscript will bring a novel strategy to synthesis of dysprosium oxide and dysprosium hydroxide nanoparticles.

* Corresponding author at: Institute of Nano Science and Nano Technology, University of Kashan, P.O. Box. 87317–51167, Kashan, I.R., Iran. Tel.: +98 361 5555333; fax: +98 361 555 2930.
E-mail address: salavati@kashanu.ac.ir (M. Salavati-Niasari).

0925-8388/$ – see front matter © 2010 Elsevier B.V. All rights reserved.
doi:10.1016/j.jallcom.2010.05.041

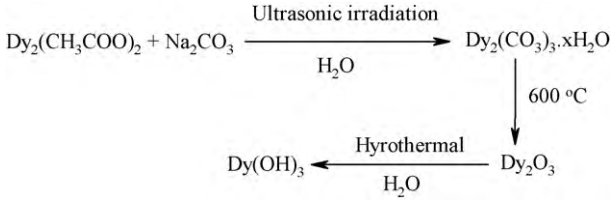

Scheme 1. Materials produced and formation methods of $Dy(OH)_3$.

2. Experimental

2.1. Materials and physical measurements

All the chemicals reagents used in our experiments were of analytical grade and were used as received without further purification. A multiwave ultrasonic generator (Sonicator 3000; Bandeline, MS 72, Germany), equipped with a converter/transducer and titanium oscillator (horn), 12.5 mm in diameter, operating at 20 kHz with a maximum power output of 600 W, was used for the ultrasonic irradiation. The ultrasonic generator automatically adjusted the power level. The wave amplitude in each experiment was adjusted as needed. XRD patterns were recorded by a Rigaku D-max C III, X-ray diffractometer using Ni-filtered Cu Kα radiation. Elemental analyses were obtained from Carlo ERBA Model EA 1108 analyzer. X-ray photoelectron spectroscopy (XPS) of the as-prepared products were measured on an ESCA-3000 electron spectrometer with nonmonochromatized Mg Kα X-ray as the excitation source. Scanning electron microscopy (SEM) images were obtained on Philips XL-30ESEM equipped with an energy dispersive X-ray spectroscopy. Transmission electron microscopy (TEM) images were obtained on a Philips EM208 transmission electron microscope with an accelerating voltage of 100 kV. Fourier transform infrared (FT-IR) spectra were recorded on Shimadzu Varian 4300 spectrophotometer in KBr pellets. Thermogravimetric-differential thermal analysis (TG-DTA) were carried out using a thermal gravimetric analysis instrument (Shimadzu TGA-50H) with a flow rate of 20.0 mL min^{-1} and a heating rate of 10 °C min^{-1} in the argon atmosphere. Room temperature photoluminescence (PL) was studied on an F-4500 fluorescence spectrophotometer.

2.2. Preparation of Dy_2O_3 nanoparticles

Dy_2O_3 nanoparticles was prepared by the reaction of $Dy_2(CH_3COO)_3$ with $NaCO_3$ in water as solvent. The reaction was performed under ultrasound power. In a typical preparation, dysprosium acetate (0.8 g) was dissolved in 25 mL of water and was irradiated with high-intensity ultrasound. A solution of $NaCO_3$ (0.8 g) in 50 mL of water was added dropwise to the $Dy(CH_3COO)_3$ solution for 15 min. The resulting white powder was filtered and washed three times with ethanol and distilled water. The washed powder was dried at 60 °C for 3 h under vacuum. Dried precipitates were calcined in air at different temperatures up to 600 °C for 2 h (Scheme 1). The molar ratio of initial materials, the time of sonicating, and the power of the ultrasound were the key parameters which were changed for more investigation. To investigate the role of surfactant on the morphology and size of nanoparticles, PEG was used as surfactant (sample 10). Table 1 shows the conditions of reactions in detail.

2.3. Preparation of $Dy(OH)_3$ nanoparticles

In a typical synthesis, 0.4 g of the obtained Dy_2O_3 nanoparticles was added to 10 mL of H_2O and then the mixture was transferred into a Teflon-lined stainless steel autoclave of 25 mL capacity. The autoclave was maintained at 120 °C for 24 h and then was allowed to cool to room temperature. The precipitated powders were separated by centrifugation, washed with deionized water and ethanol for three times, and then dried in a vacuum oven at 50 °C for 4 h (Scheme 1).

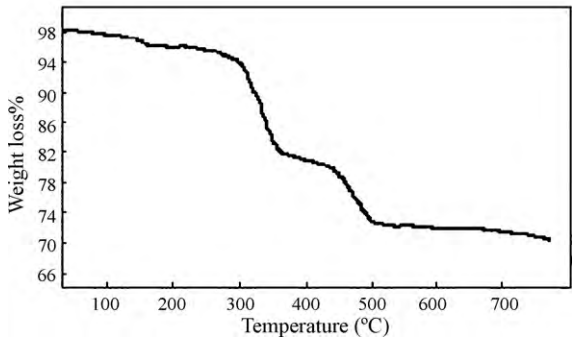

Fig. 1. Thermogravimetric patterns of sample no. 1.

3. Results and discussion

Fig. 1a shows the TGA curve of the as-prepared carbonate, sample no. 1, in argon atmosphere from ambient temperature to 800 °C. The TGA curve shows three step weight loss, at ca. 120 °C (weight loss ~ 2.8%), at ca. 500 °C (weight loss ~ 18.4%) and at ca. 600 °C (weight loss ~ 9.7%) with an overall weight loss of 30.9%, which is due to the evaporation of H_2O molecules in the sample, and then evolution of CO_2 during the thermal decomposition. Studies on the thermal behavior of the as-prepared carbonate, sample no. 1, showed features similar to those observed for other lanthanum carbonates such as $La_2(CO_3)_3{\cdot}8H_2O$, $La_2(CO_3)_3{\cdot}1.4H_2O$, $La_2(CO_3)_2(OH)_2{\cdot}H_2O$, $La_2(CO_3)_3$, etc. [19–21]. Here, according to above references, we concluded that dysprosium carbonates can be similar to lanthanum carbonates [22].

XRD analysis, which is the most useful technique for identification of crystalline structure, was employed to investigate the prepared sample. In Fig. 2a, the X-ray diffraction pattern of sample no. 1 is shown. This diffraction pattern it is similar to the XRD pattern for $Dy_2(CO_3)_3{\cdot}XH_2O$ reported by Philippini et al. [23]. In Fig. 2a, it is noted that the full width at half maximum (FWHM) of the diffraction peak at about 22° (2θ) is obviously narrow than that of others in the same pattern. The different FWHM may suggest that these diffraction peaks are not attributed to the same phase of dysprosium carbonate. It is possible that, some impurity such as hydroxycarbonate can be produced under current synthetic condition. Some other spectroscopic data can confirmed this issue that has been reported in FT-IR spectra. The XRD results for the samples no. 3 and 4 are shown in Fig. 2b and c, respectively. Annealing the samples at 600 °C resulted in the formation of two crystalline phases, namely dysprosium oxide and dysprosium oxide carbonate (Fig. 2b), which is in agreement with Hussein et al. [24]. As shown in

Table 1
Experimental condition for the preparation of $Dy_2(CO_3)_3$, Dy_2O_3 and $Dy(OH)_3$.

Sample no.	Na_2CO_3 (g)	$Dy(OAC)_3$ (g)	Time of sonication (min)	Temperature of calcination	Time and temperature of hydrothermal
1	0.8	0.8	15	–	–
2	0.8	0.8	15	600 °C for 2 h	–
3	0.8	0.8	15	650 °C for 2 h	–
4	0.8	0.8	15	650 °C for 2 h	24 h (120 °C)
5	0.8	0.8	30	500 °C for 2 h	–
6	0.8	0.8	30	700 °C for 2 h	–
7	0.8	0.8	30	750 °C for 2 h	–
8	0.8	0.8	30	800 °C for 2 h	–
9	0.8	0.8	30	850 °C for 2 h	–
10	0.8	0.8 + 3 mL PEG	15	650 °C for 2 h	–
11	0.8	0.8	10	–	–
12	0.8	0.8	20	–	–

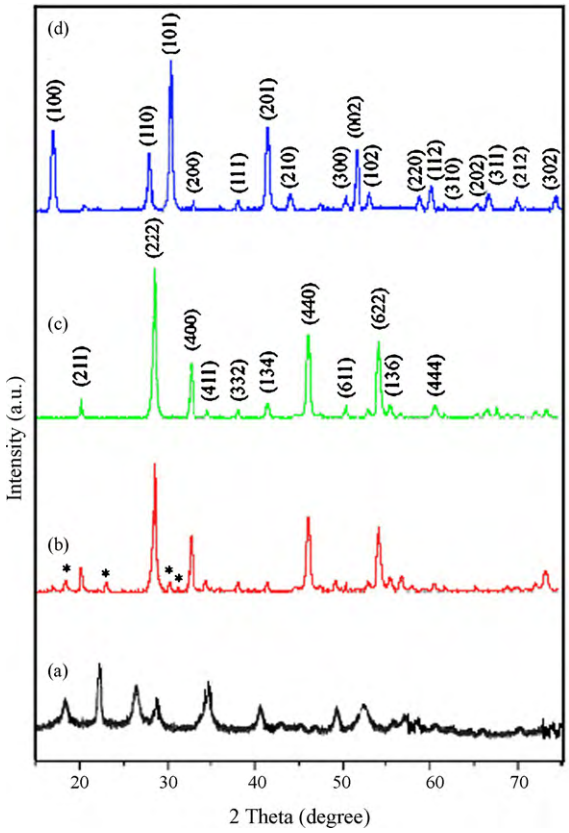

Fig. 2. XRD patterns of (a) dried precipitate (sample no. 1), (b) calcined at 600 °C (sample no. 2), (c) calcined at 650 °C (sample no. 3), and (d) hydrothermal method (sample no. 4).

Fig. 2c, the XRD pattern of the pure Dy_2O_3 reveals that the diffractogram can be determined as Dy_2O_3 with cubic bixbyite phase, also known as the C-rare-earth sesquioxide structure (lattice constant a of cubic unit cell: 1.0670 nm), owing to diffraction peaks, which can be filed to (2 1 1), (2 2 2), (4 0 0), (4 1 1), (3 3 2), (1 3 4), (4 4 0), (6 1 1), (6 2 2), (1 3 6) and (4 4 4) planes (JCPDS Card No. 86-1327). No other peak exists in the Fig. 2c, showing the high purity and well crystallinity of the samples. From XRD data Fig. 2c, the crystallite size (D_c) of the as-prepared Dy_2O_3, sample no. 3, was calculated to be 10 nm using the Scherrer equation [25],

$$D_c = \frac{K\lambda}{\beta \cos\theta}$$

where β is the breadth of the observed diffraction line at its half-intensity maximum, K is the so-called shape factor, which usually takes a value of about 0.9, and λ is the wavelength of X-ray source used in XRD. The average size of the particles of sample no. 3 was 10 nm, which is to some extent in agreement with that observed from SEM and TEM images.

The XRD pattern of the obtained $Dy(OH)_3$ product is shown in Fig. 2d. All of the peaks can be readily indexed to a pure hexagonal phase ($P63/m$ (1 7 6)) of $Dy(OH)_3$ with lattice constants a = 6.280 Å and c = 3. 570 Å (JCPDS 19–0430). Diffraction peaks, which can be filed to (1 0 0), (1 1 0), (1 0 1), (2 0 0), (1 1 1), (2 0 1), (2 1 0), (3 0 0), (0 0 2), (1 0 2), (2 2 0), (1 1 2), (3 1 0), (2 0 2), (3 1 1), (2 1 2) and (3 0 2) planes (JCPDS Card No. 19–0430) are labeled in Fig. 2d. This pattern can prove this point that pure $Dy(OH)_3$ was successfully prepared by hydrolysis of Dy_2O_3 via hydrothermal process.

TEM photograph of the products have been given in Fig. 3. Fig. 3a and b shows TEM images of $Dy_2(CO_3)_3{\cdot}xH_2O$, sample no. 1, and $Dy_2(CO_3)_3$, sample no. 3. The sizes of nanoparticles obtained from the XRD diffraction patterns are in close agreement with the TEM studies which show sizes of 10–15 nm for sample no. 3. Their shapes are nearly spherical. To investigate the size distribution of the nanoparticles particle size histograms were prepared for sam-

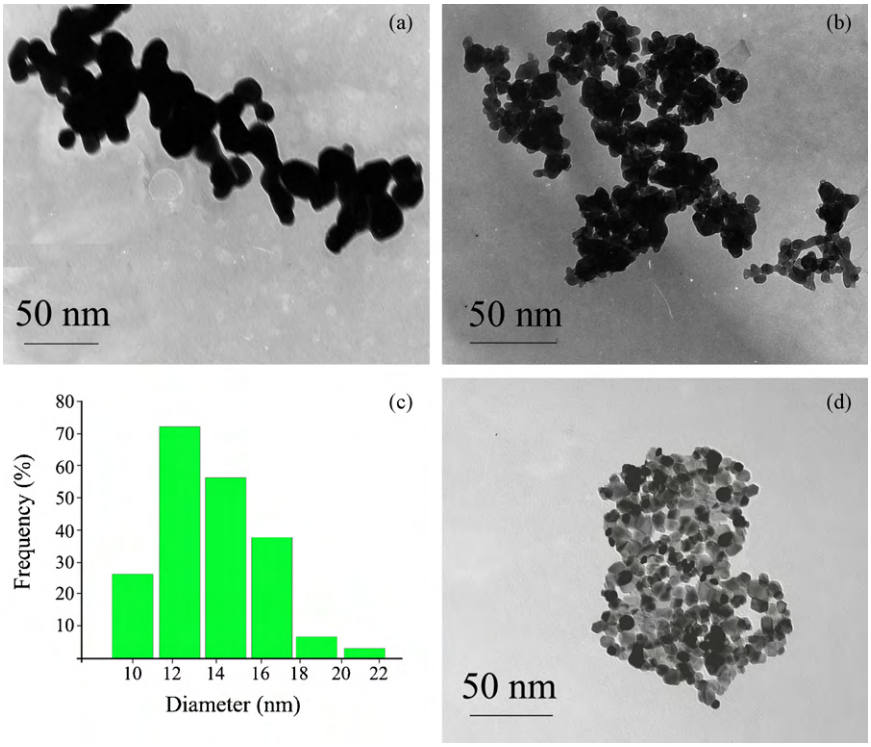

Fig. 3. SEM images of (a) dried precipitate (sample no. 1), (b) calcined at 650 °C (sample no. 3), (c) size distribution histogram of calcined sample at 650 °C (sample no. 3), and (d) hydrothermal method (sample no. 4).

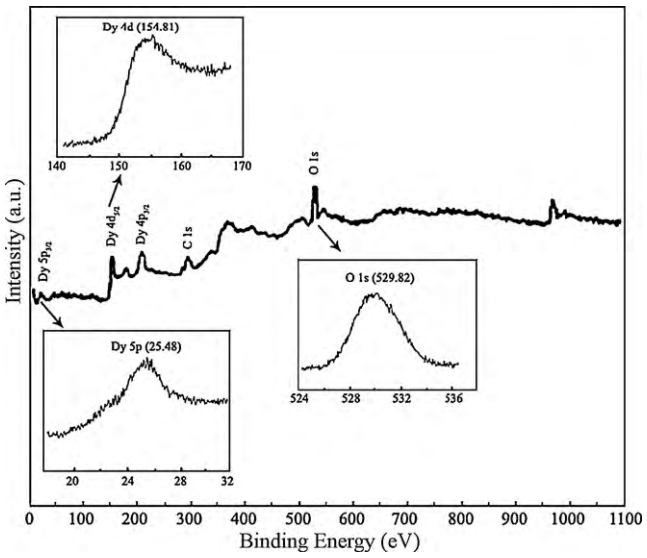

Fig. 4. XPS spectra of the as-synthesized products, (sample no. 3): survey spectrum; Dy 5p region; Dy 4d region; and O 1s region.

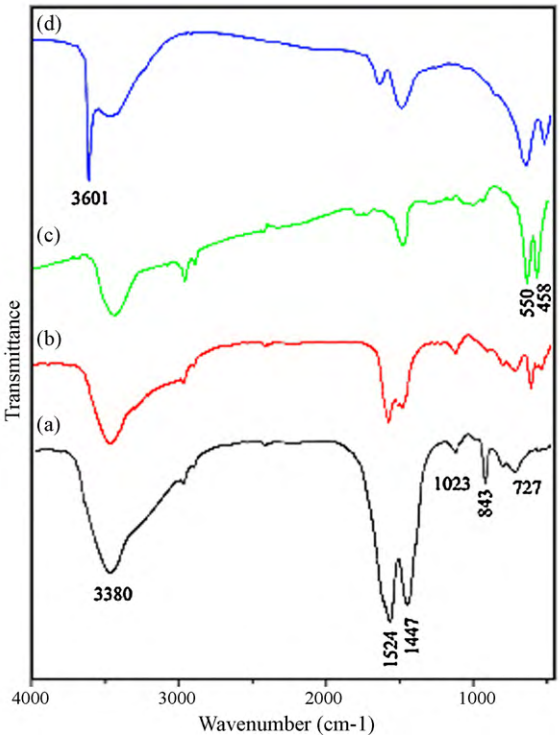

Fig. 5. FT-IR spectra of the as-synthesized products: (a) dried precipitate (sample no. 1), (b) calcined at 600 °C (sample no. 2), (c) calcined at 650 °C (sample no. 3), and (d) hydrothermal method (sample no. 4).

ple no. 3 (Fig. 3c). This size distribution is centered at a value of 12 nm. Fig. 3d shows TEM image of $Dy_2(OH)_3$ nanoparticles, sample no. 4. The average particle size of $Dy_2(OH)_3$ was about 14 nm.

Further evidence for the composition was illuminated by the XPS of the Dy_2O_3 (sample no. 3). The binding energies obtained in the XPS analysis were corrected for specimen by referencing the C 1s to 284.55 eV. The survey XPS spectrum of the product (Fig. 4) suggests that there are no other metal elements on the surface of the sample except for Dy. Fig. 4 shows that the binding energy of Dy 5p and Dy 4d, are 25.48 and 154.81 eV, respectively. In Fig. 4, it can be seen that the O 1s profile is asymmetric, indicating that two oxygen species are present in the nearby region. The peak at about 529.82 eV can be indexed to the O^{2-} in the Dy_2O_3 [22].

FT-IR spectroscopy is a useful tool to understand the functional group of any organic molecule. The infrared spectra of dried precipitate (sample no. 1) and calcined samples at different temperatures are shown in Fig. 5. The absorption peak at 3380 cm^{-1} in Fig. 5a is attributed to the stretching vibration of the O–H bond and the bending vibration of H–O–H from water molecules on the external surface of the samples during handling to record the spectra [26–30]. One can be observed a broad band located between 3800 and 3200 cm^{-1} and can be attributed to the some hydroxycarbonate impurity. The absorption bands at 1524 and 1447 cm^{-1} are attributed to the υ_3 mode of CO_3^{2-} group. The splitting of the band could be due to the carbonate ions located at a crystallographically non-equivalent site [31]. The absorption bands at 1023, 843, and 727 cm^{-1} are assigned to the υ_1, υ_2, and υ_4 modes of the carbonate ion, respectively [32,33]. Calcination of the precipitates to 500 °C, (sample no. 5), did not result in any change the IR spectra, with the exception of a reduction in intensity of the hydroxyl group, which again supports the idea of the evaporation of adsorbed water at 100 °C. Upon further heating to 600 °C, (sample no. 2), the absorption band of carbonate ions were reduced and the absorption band of cubic phase Dy_2O_3 appears at 550 cm^{-1} and 458 cm^{-1} (Fig. 5b). This is in agreement with the corresponding XRD spectrum where reflections for dysprosium oxide and weak reflections of dysprosium oxide carbonate were observed together. Further calcination of the precipitates to 650 °C, (sample no. 3), eliminates the presence of carbonate ions completely and the absorption band of Dy_2O_3 appears at 550 cm^{-1} and 458 cm^{-1} (Fig. 5c). In this temperature there were no additional peaks observed in the corresponding XRD spectrum except cubic Dy_2O_3. So pure dysprosium oxide can be obtained by calcination of the precipitate at 650 °C, and no other absorption band was observed in the spectrum. According to Fig. 5d after hydrolysis of Dy_2O_3 via hydrothermal process a sharp peaks at 3601 cm^{-1} are assigned for stretching mode of OH^- in $Dy(OH)_3$, (sample no. 4), was appeared.

The energy dispersive spectrometry (EDS) analysis was employed to determine the composition of Dy_2O_3, (sample no. 3), and $Dy(OH)_3$, (sample no. 4), nanoparticles. As shown in Fig. 6a, the EDS clearly identify that the nanoparticles are composed of O and Dy, with the molar ratio of about 3:2 (O/Dy), they should therefore be attributed to Dy_2O_3. As shown in Fig. 6b, only oxygen and dysprosium elements existed in the nanoparticles with the molar ratio of about 3 (O/Dy). Taking into consideration of H, they should therefore be attributed to $Dy(OH)_3$.

In addition, some other conditions were examined to investigate the morphology of products, if any, and compare them with each other. The relationship between the mean particle size of Dy_2O_3 and calcination temperature is plotted in Fig. 7 when the calcination time is 2 h. The result shows that the mean particle size increases with increasing calcination temperature. It grows slowly at lower temperature, and increases very quickly when the temperature is beyond 750 °C. Fig. 8 shows SEM images of the dysprosium oxide nanoparticles calcined at 700, 750, 800, and 850 °C for 2 h, respectively. Quasi-spherical nanoparticles are observed when the calcinations temperature is below 750 °C. At 800 °C, the particles have begun to agglomerate and grow up. When the temperature reaches to 850 °C, all particles have been sintered completely together leading to the formation of big particles [34]. The particle size is 20–30 nm at 700 °C, 30–40 nm at 750 °C, 70–80 nm at 800 °C and about 100–150 nm at 850 °C. Hence, the optimum calcinations temperature is 650 °C and Dy_2O_3 nanoparticles with spherical shape prepared by the above method has 10–15 nm particle size.

To investigate the role of PEG on the morphology of Dy_2O_3 nanoparticles, one of the reactions was performed in the presence

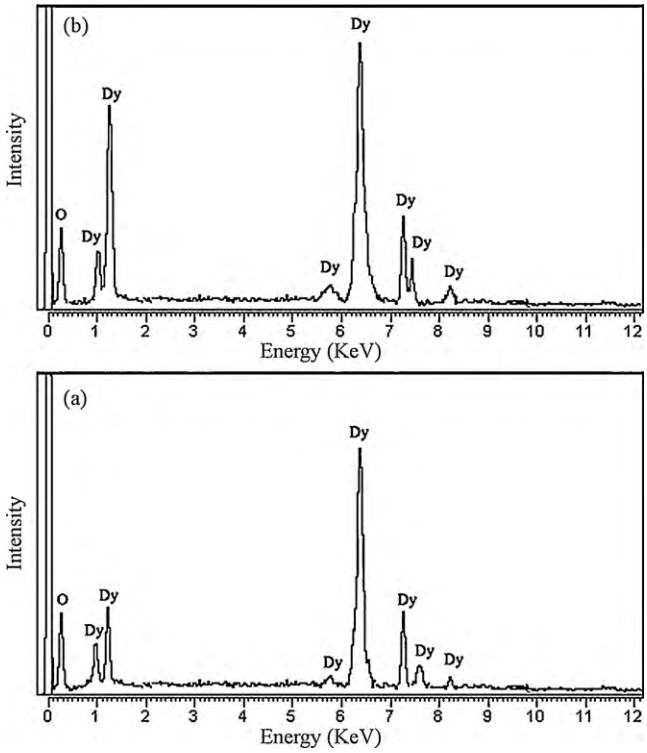

Fig. 6. EDS patterns of (a) Dy_2O_3, (sample no. 3), and (b) $Dy(OH)_3$, (sample no. 4), nanoparticles.

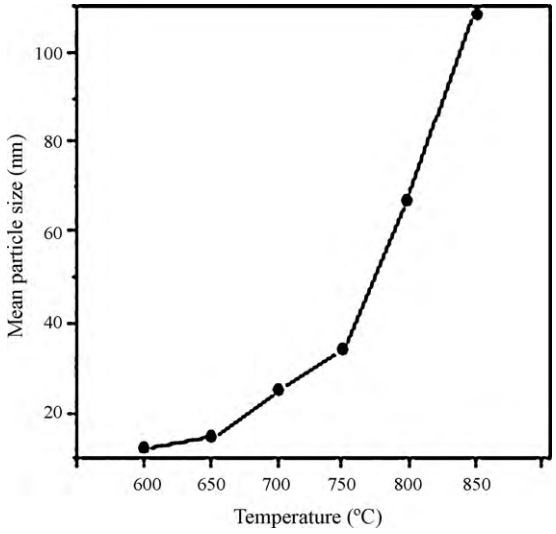

Fig. 7. The mean particle size of Dy_2O_3 nanoparticles as a function of calcination temperature.

of PEG (sample no. 10). PEG is a long-chain polymer and helps to form one-dimensional (1D) Dy_2O_3 nanostructures [35]. Fig. 9 shows the SEM image of sample no. 10. It has been reported [36,37] that the presence of a capping molecule (such as PEG) can alter the surface energy of crystallographic surfaces, in order to promote the anisotropic growth of the nanocrystals. In this work PEG adsorbs on the crystal nuclei and its helps the nanoparticles to grow separately.

For investigating the effect of sonication time on the morphology of the products, the reaction carried out in 10 and 20 min. As it is shown in Fig. 10, with decreasing of aging time to 10 min (sample no. 11), the obtained particles were bigger than the particles of sample no. 1 with the aging time of 15 min. With increasing of the aging time to 20 min (sample no. 12) the nanoparticles with average size of 40 nm in diameter is produced.

It is known that lanthanide oxides are ideal hosts for photoluminescence [38] and pure lanthanide oxides seldom radiate luminescence according to luminescence theory of rare-earth atoms [39]. For understanding PL property of Dy_2O_3, one of the prepared samples (sample no. 3) was applied for this proposes. In

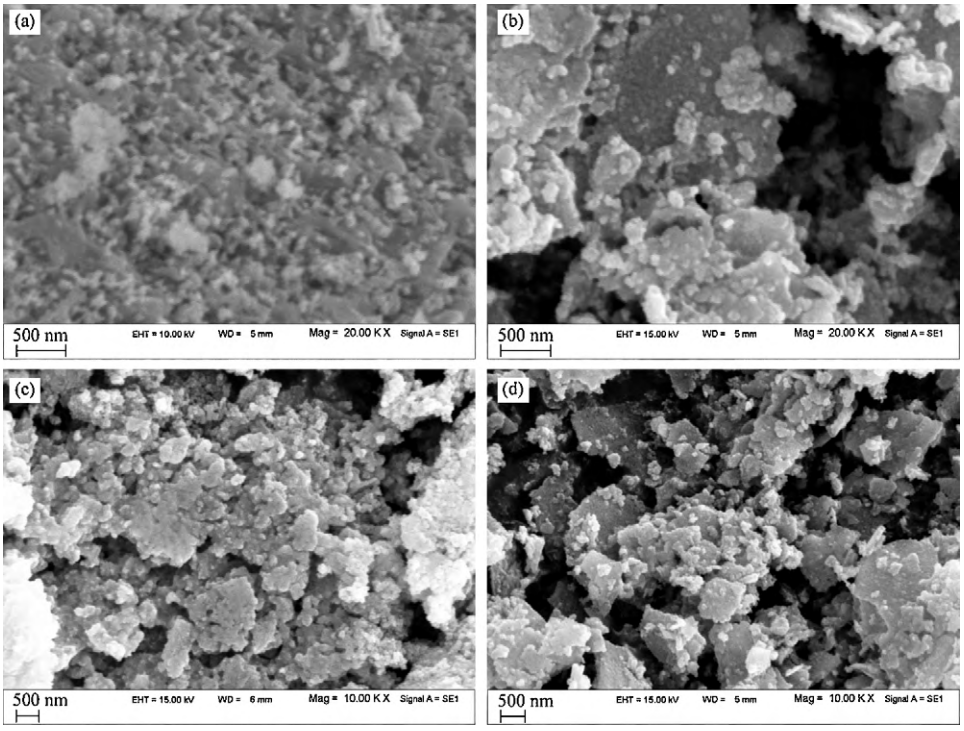

Fig. 8. SEM images of the Dy_2O_3 nanoparticles calcined at (a) 700 °C (sample no. 6), (b) 750 °C (sample no. 7), (c) 800 °C (sample no. 8), and (d) 850 °C (sample no. 9).

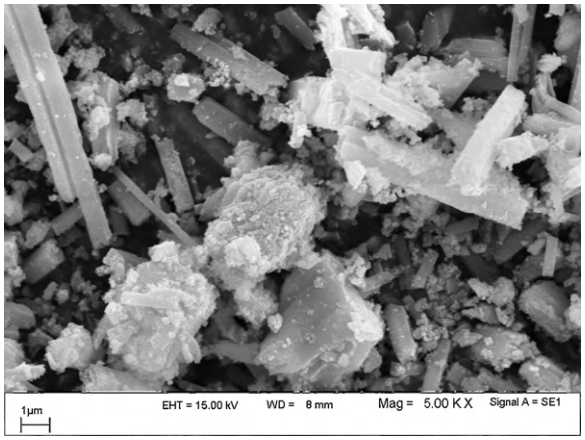

Fig. 9. SEM image of the Dy_2O_3 nanoparticles prepared at the presence of PEG (sample no. 10).

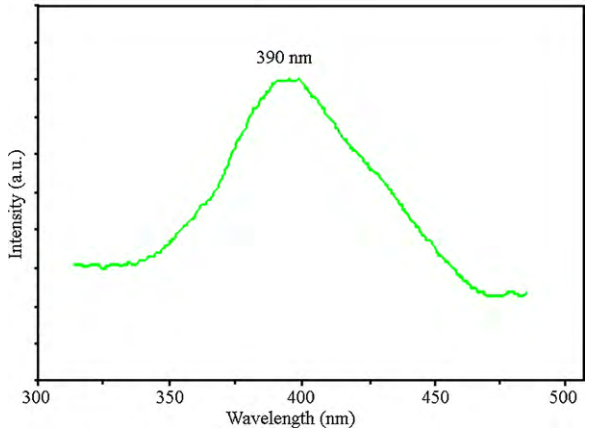

Fig. 11. Photoluminescence spectra of Dy_2O_3 nanoparticles (sample no. 3).

Fig. 11 a green emission band at about 390 nm was observed at excitation wavelength of 300 nm. The green emission band may attribute to recombination of a delocalized electron close to the conduction band with a single charged state of surface oxygen vacancy, according to Wang's proposal [40]. It is known that the fluorescence of rare-earth ions mainly comes from the interior electron transitions of the 4f shell, but the 4f shell of Dy^{3+} is empty and no f–f transitions exist in our products. Herein, the emission spectrum of the Dy_2O_3 nanoparticles consists of a broad band located between 320 and 470 nm and can be attributed to the self-trapped exciton luminescence [41]. Many of the free holes and free electrons were created after the lattice was irradiated, and the self-trapped exciton luminescence can be formed directly from electron–hole pairs. During the diffusion of the self-trapped exciton luminescence, they can be an irradiative recombination, leading to luminescence, the possible origin of the visible PL [42].

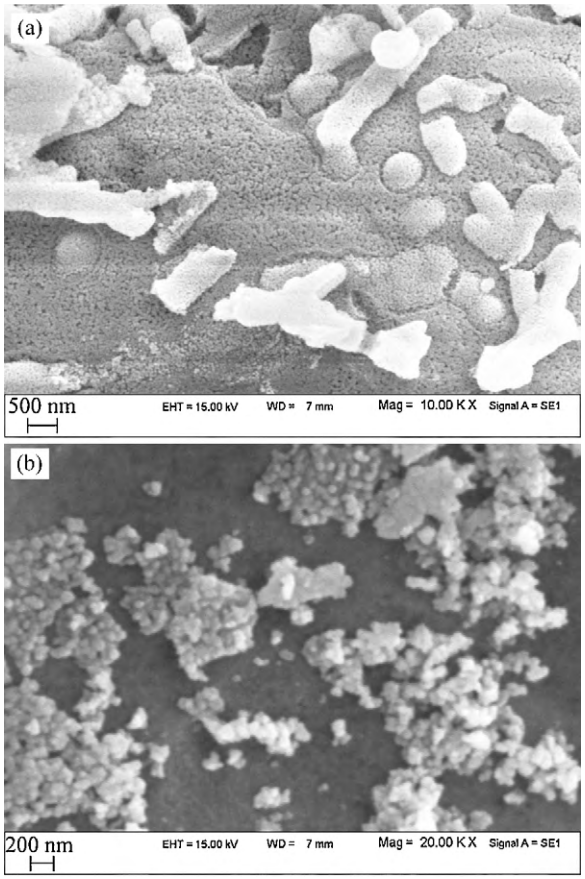

Fig. 10. SEM images of as-prepared nanoparticles: (a) sample no. 11 and (b) sample no. 12.

4. Conclusion

In summary, $Dy_2(CO_3)_3{\cdot}xH_2O$ nanoparticles were synthesized by a sonochemical method. This method brings forward a broad idea to synthesize other rare-earth compounds with various morphologies and novel properties. Dysprosium oxide with high purity was obtained from calcinations of $Dy_2(CO_3)_3{\cdot}xH_2O$ nanoparticles at 650 °C for 2 h. In summary, we have found a simple route to prepare $Dy(OH)_3$ nanoparticles by facile hydrothermal method of Dy_2O_3. The XRD, TEM, SEM, XPS, FT-IR were used to characterize the products and the PL properties of pure Dy_2O_3 nanoparticles were discussed. The effect of some parameters such as, calcinations temperature and addition of PEG as surfactant on the size and morphology of the obtained products were investigated.

Acknowledgement

Authors are grateful to the council of University of Kashan for their unending efforts to provide financial support to undertake this work.

References

[1] M. Kamruddin, P.K. Ajikumar, R. Nithya, A.K. Tyagi, B. Raj, Scripta Mater. 50 (2004) 417–422.
[2] M. Salavati-Niasari, F. Davar, Mater. Lett. 63 (2009) 441–443.
[3] M. Salavati-Niasari, F. Davar, M.R. Loghman-Estarki, J. Alloys Compd. 494 (2010) 199–204.
[4] F. Davar, Z. Fereshteh, M. Salavati-Niasari, J. Alloys Compd. 476 (2009) 797–801.
[5] M. Salavati-Niasari, D. Ghanbari, F. Davar, J. Alloys Compd. 488 (2009) 442–447.
[6] A.-W. Xu, Y.-P. Fang, L.-P. You, H.-Q. Liu, J. Am. Chem. Soc. 125 (2003) 1494–1495.
[7] Shu Yin, Shingo Aktia, Makoto Shinozaki, Ruixing Li, Tsugo Sato, J. Mater. Sci. 43 (2008) 2234–2239.
[8] G. Wang, Z. Wang, Y. Zhang, G. Fei, L. Zhang, Nanotechnology 15 (2004) 1307–1311.
[9] T. Sreethawong, S. Chavadej, S. Ngamsinlapasathian, S. Yoshikawa, J. Colloid Interface Sci. 300 (2006) 219–224.
[10] X.C. Song, Y.F. Zheng, Y. Wang, Mater. Res. Bull. 43 (2008) 1106–1111.
[11] K.S. Suslick, S.B. Choe, A.A. Cichowlas, M.W. Grinstaff, Nature 353 (1991) 414–416.
[12] H. Wang, Y.N. Lu, J.J. Zhu, H.Y. Chen, Inorg. Chem. 42 (2003) 6404–6411.
[13] X.W. Zheng, Y. Xie, L.Y. Zhu, X.C. Jiang, A.H. Yan, Ultrason. Sonochem. 9 (2002) 311–314.
[14] L.Z. Zhang, J.C. Yu, Chem. Commun. (2003) 2078–2079.
[15] V.G. Pol, O. Palchik, A. Gedanken, I. Felner, J. Phys. Chem. B 106 (2002) 9737–9743.

[16] R. Katoh, Y. Tasaka, E. Sekreta, M. Yumura, F. Ikazaki, Y. Kakudate, S. Fujiwara, Ultrason. Sonochem. 6 (1999) 185–187.
[17] B. Gates, B. Mayers, A. Grossman, Y.N. Xia, Adv. Mater. 14 (2002) 1749–1752.
[18] A. Gedanken, Ultrason. Sonochem. 11 (2004) 47–55.
[19] M.L. Panchula, M. Akinc, J. Eur. Ceram. Soc. 16 (1996) 833–841.
[20] S. Hamada, Y. Kudo, H. Matsuda, Bull. Chem. Soc. Japan 66 (1993) 2402–2406.
[21] K. Foger, M. Hoang, T.W. Turney, J. Mater. Sci. 27 (1992) 77–82.
[22] K. Han, Y. Zhang, T. Cheng, Z. Fang, M. Gao, Z. Xu, X. Yin, Mater. Chem. Phys. 114 (2009) 430–433.
[23] V. Philippini, T. Vercouter, A. Chaussé, P. Vitorge, J. Solid State Chem. 181 (2008) 2143–2154.
[24] G.A.M. Hussein, W.J. Kroenke, B. Goda, K. Miyaji, J. Anal. Appl. Pyrol. 39 (1997) 35–51.
[25] R. Jenkins, R.L. Snyder, Chemical Analysis: Introduction to X-ray Powder Diffractometry, John Wiley & Sons, Inc., New York, 1996, p. 90.
[26] M. Salavati-Niasari, F. Davar, Z. Fereshteh, J. Alloys Compd. 494 (2010) 410–414.
[27] M. Salavati-Niasari, F. Davar, M. Farhadi, J. Sol–Gel Sci. Technol. 51 (2009) 48–52.
[28] F. Mohandes, F. Davar, M. Salavati-Niasari, J. Magn. Magn. Mater. 322 (2010) 872–877.
[29] M. Salavati-Niasari, N. Mir, F. Davar, J. Alloys Compd. 476 (2009) 908–912.
[30] M. Salavati-Niasari, N. Mir, F. Davar, J. Alloys Compd. 493 (2010) 163–168.
[31] A.I.Y. Tok, L.T. Su, F.Y.C. Boey, S.H. Ng, J. Nanosci. Nanotechnol. 7 (2007) 1–90.
[32] D.L. Zhao, Q. Yang, Z.H. Han, J. Zhou, S.B. Xu, F.Y. Sun, Solid State Sci. 10 (2008) 31–39.
[33] P. Jeevanandam, Y. Koltypin, O. Palchik, A. Gedanken, J. Mater. Chem. 11 (2001) 869–873.
[34] X. Wang, M. Wang, H. Song, B. Ding, Mater. Lett. 60 (2006) 2261–2265.
[35] W.Z. Wang, G.H. Wang, X.S. Wang, Y.J. Zhan, Y.K. Liu, C.L. Zheng, Adv. Mater. 14 (2002) 67–69.
[36] W.I. Park, D.H. Kim, S.W. Jung, G.C. Yi, Appl. Phys. Lett. 80 (2002) 4232–4234.
[37] J. Du, Z. Liu, Y. Huang, Y. Gao, B. Han, W. Li, G. Yang, J. Cryst. Growth 280 (2005) 126–134.
[38] L. Yu, H. Song, Z. Liu, L. Yang, S. Lu, Phys. Chem. Chem. Phys. 8 (2006) 303.
[39] J.Y. Li, Luminescent Materials of Rare Earths and their Applications, Chemical Industry, Beijing, 2003, p. 15.
[40] C. Hu, H. Liu, W. Dong, Y. Zhang, G. Bao, C. Lao, Z.L. Wang, Adv. Mater. 19 (2007) 470–474.
[41] Y. Zhang, K. Han, T. Cheng, Z. Fang, Inorg. Chem. 46 (2007) 4713–4717.
[42] Y. Pei, X.F. Chen, R.H. Mao, G.H. Ren, J. Cryst. Growth 279 (2005) 390–393.